ACS NANO

www.acsnano.org

ARTICLE

Chiral Stacking Identification of Two-Dimensional Triclinic Crystals Enabled by Machine Learning

He Hao, Kangshu Li, Xujing Ji, Xiaoxu Zhao, Lianming Tong,* and Jin Zhang

Cite This: *ACS Nano* 2024, 18, 13858−13865

Read Online

ACCESS | Metrics & More | Article Recommendations | Supporting Information

ABSTRACT: **Chiral materials possess broken inversion and mirror symmetry and show great potential in the application of next-generation optic, electronic, and spintronic devices. Two-dimensional (2D) chiral crystals have planar chirality, which is nonsuperimposable on their 2D enantiomers by any rotation about the axis perpendicular to the substrate. The degree of freedom to construct vertical stacking of 2D monolayer enantiomers offers the possibility of chiral manipulation for designed properties by creating multilayers with either a racemic or enantiomerically pure stacking order. However, the rapid recognition of the relative proportion of two enantiomers becomes demanding due to the complexity of stacking orders of 2D chiral crystals. Here, we report the unambiguous identification of racemic and enantiomerically pure stackings for layered $ReSe_2$ and ReS_2 using circular polarized Raman spectroscopy. The chiral Raman response is successfully manipulated by the enantiomer proportion, and the stacking orders of multilayer $ReSe_2$ and ReS_2 can be completely clarified with the help of second harmonic generation and scanning transmission electron microscopy measurements. Finally, we trained an artificial intelligent Spectra Classification Assistant to predict the chirality and the complete crystallographic structures of multilayer $ReSe_2$ from a single circular polarized Raman spectrum with the accuracy reaching 0.9417 ± 0.0059.**

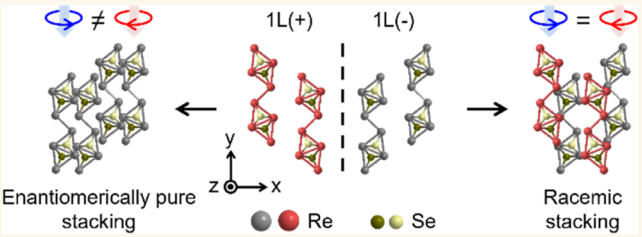

KEYWORDS: *2D chiral crystals, stacking order, enantiomer proportion, circular polarized Raman spectroscopy, machine learning*

INTRODUCTION

A chiral object is not superimposable to its mirror image (enantiomer), which renders chiral enantiomer functionalities in intermolecular recognition[1] and assembling,[2] electron spin manipulation,[3,4] and circularly polarized light−matter interaction.[5] For a system containing both chiral enantiomers, its chiral properties can be manipulated by the relative proportions of the two enantiomers. Taking chiral molecules as examples, the solution with both enantiomers in equal amounts, known as a racemic mixture (RM), is optically inactive and has negligible chiroptical response; while a solution with an unequal amount of enantiomers normally preserves optical activity, which can be roughly treated as the superposition of an optically inactive racemic mixture and the optically active enantiomerically pure (EP) remainder.[6] Recently, a few two-dimensional (2D) layered crystals including ReS_2, $ReSe_2$,[7−9] and 1T-TaS_2[10−13] are reported to have 2D planar chirality,[14] which present numerous chiral properties such as chiral charge density wave order,[10,12] enantiomer-dependent second harmonic generation (SHG),[11] and linear polarized Raman[8,9] response, as well as quantum interference-directed chiral Raman scattering.[7] Although these materials are achiral in three-dimensional space, they are usually confined to a substrate (xy-plane) and are therefore nonsuperimposable on their 2D enantiomers by any rotation about the axis perpendicular to the plane [see the example of monolayer (1L) ReX_2 (X = S or Se) in Figure 1a]. When two monolayer 2D chiral crystals are stacked together, a 2D enantiomer mixture is formed, and its chirality-related properties should depend on the relative proportion of the two enantiomers. As shown in Figure 1b, if the top and bottom monolayers have the same 2D chirality, they generate an "EP stacking," and the resulting bilayer should have a similar chiroptical response as the monolayer. For bilayers containing a monolayer with different 2D chirality, they have a "racemic stacking" and should not exhibit chiroptical phenomena (Figure 1c). Therefore, one can expect that the chirality-related

Received: March 1, 2024
Revised: April 30, 2024
Accepted: May 7, 2024
Published: May 14, 2024

https://doi.org/10.1021/acsnano.4c02898
ACS Nano 2024, 18, 13858−13865

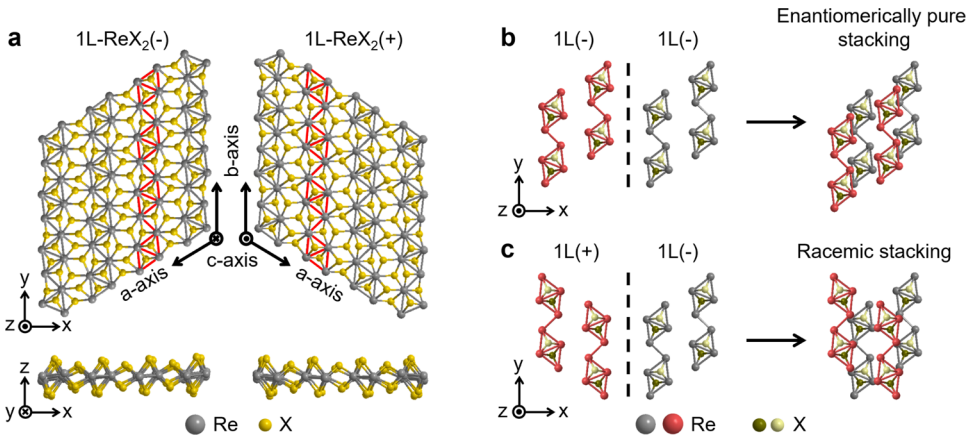

Figure 1. Racemic and enantiomerically pure stackings of ReX_2 (X = S or Se). (a) Top view (top row) and side view (bottom row) of monolayer ReX_2 enantiomers, which are named 1L- ReX_2(+) and 1L- ReX_2(−). The Re-chains are marked in red. The substrate plane is the xy-plane. (b, c) Simplified crystal structures of enantiomerically pure stacking (b) and racemic stacking (c) of bilayer ReX_2. Only Re atoms and a part of the X atoms are shown for clarity. The Re atoms in different 1L-ReX_2 are marked in different colors (red or gray). The X atoms above and below the plane of Re atoms are colored in light yellow and dark yellow, respectively. Similar crystal structure representations will be used in the rest of this paper.

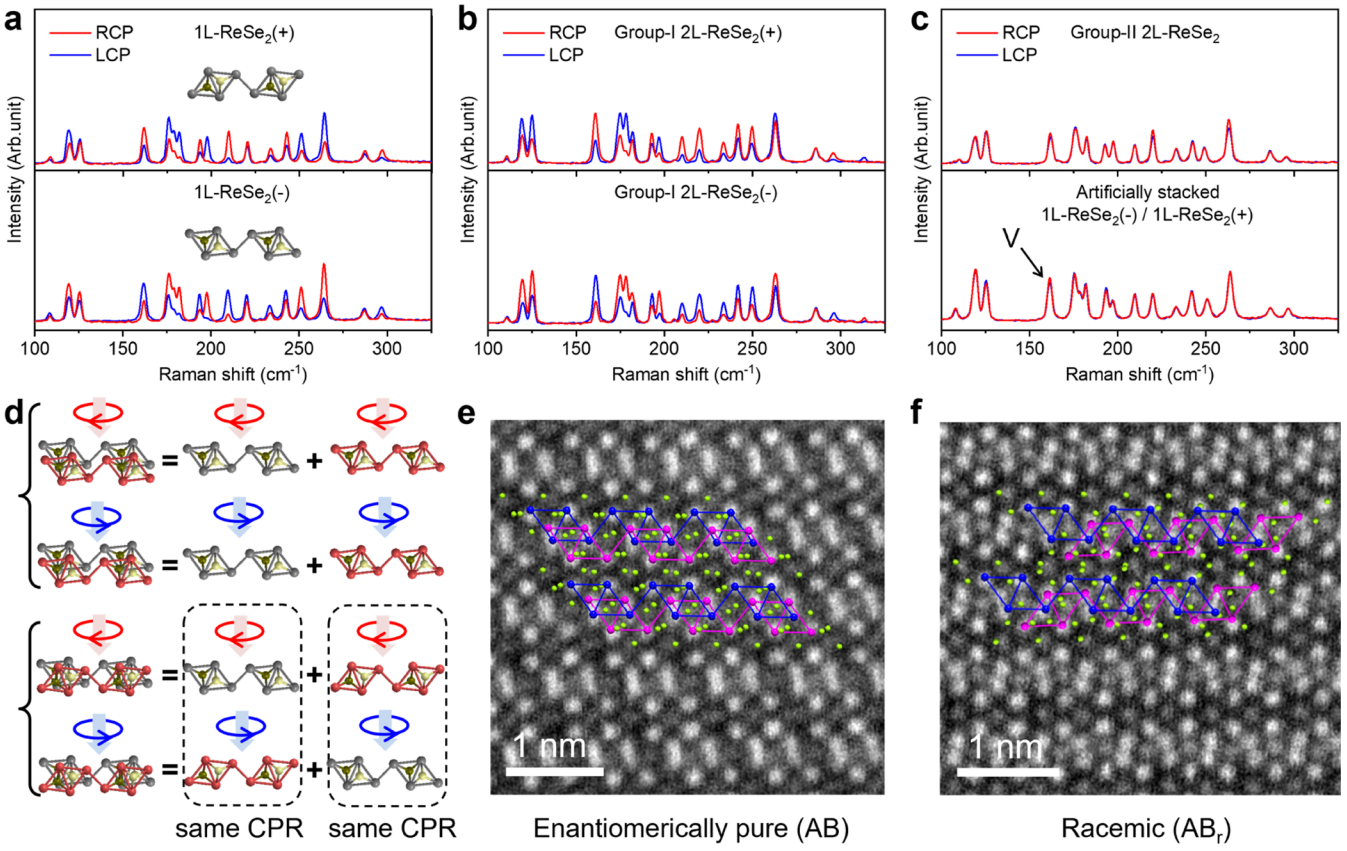

Figure 2. Enantiomer proportions and stacking orders of bilayer $ReSe_2$. (a−c) Circularly polarized Raman spectra of the monolayer (a), Group-I bilayer (b), and Group-II bilayer (c) $ReSe_2$. (+) and (−) denote different 2D chirality. The insets of (a) depict the simplified crystal structures of 1L-$ReSe_2$(+) and 1L-$ReSe_2$(−). The spectra of an artificially stacked 1L-$ReSe_2$(+)/1L-$ReSe_2$(−) sample are also shown in (c) with mode V marked as "V." (d) Schematic diagram of CPR intensity superposition theory for enantiomerically pure-stacked (top two rows) and racemic-stacked (top two rows) 2L-$ReSe_2$. The red (blue) arrows pointing clockwise (anticlockwise) represent RCP (LCP) excitations. (e, f) annular dark-field (ADF)-STEM images of Group-I (e) and Group-II (f) 2L-$ReSe_2$ overlain with the proposed atomic structural models. The Re-chains of different layers are marked with different colors (blue or purple). Scale bar: 1 nm.

properties of multilayer 2D chiral crystals, such as chiral charge density wave and chiral Raman scattering, can be manipulated by the stacking order and enantiomer proportion degrees of freedom.

Despite the possibility of constructing EP and racemic stackings of 2D chiral crystals, the stacking orders from the point of view of the enantiomer mixture have not been discussed so far. Particularly, the correct stacking of many 2D chiral

https://doi.org/10.1021/acsnano.4c02898
ACS Nano 2024, 18, 13858−13865

crystals is under debate even for mechanically exfoliated samples.[15−21] Taking mechanically exfoliated ReS_2 as an example, the controversies in stacking orders result in different atomic structures extracted from scanning transmission electron microscopy (STEM)[18,21] and different layer number dependence of SHG intensities.[22,23] These facts make the identification of the enantiomer proportion degree of freedom in the stacking order even more challenging. Therefore, a proper and efficient method to evaluate the enantiomer proportion is greatly desired, not only for the stacking order determination but also for the chirality manipulation of multilayer 2D chiral crystals.

Herein, we report the unambiguous measurement of enantiomer proportion in mechanically exfoliated layered $ReSe_2$ and ReS_2 using circular polarized Raman (CPR) spectroscopy. We find two distinct stacking orders in bilayer (2L)-$ReSe_2$, namely, EP and racemic stackings. The former shows different Raman spectroscopic features under left- and right-handed light excitation, while identical Raman spectra appear in the latter. The chiral Raman response for multilayers is sensitively dependent on the enantiomer proportion. Then, the complete stacking orders of multilayer ReX_2, considering the possible relative translation, in-plane rotation, and 2D chirality, are revealed by using a systematic method combining CPR, SHG, and STEM. Finally, we trained an AI Spectra Classification Assistant (AI-SCAN) based on a machine learning model, which can instantly predict the layer number, stacking order, and 2D chirality of mL-ReX_2 from a single CPR spectrum with the cross-validation (CV) accuracy reaching 0.9417 ± 0.0059. The above results show the potential of using stacking order and enantiomer proportion degrees of freedom for 2D chirality manipulation and will benefit the research of the chirality-dependent properties of 2D chiral crystals as well as the rapid characterization of the stacking order of 2D materials.

RESULTS AND DISCUSSION

Racemic and EP Stackings of Bilayer $ReSe_2$. In this work, single crystals of $ReSe_2$ and ReS_2 are purchased from HQ graphene, and the few-layers are mechanically exfoliated on 90 nm SiO_2/Si substrates. The optical setup for circularly polarized Raman spectroscopy is identical to the previous report.[7] The layer numbers of exfoliated samples are determined by the frequencies of their interlayer Raman modes (Figure S1).[24] As shown in Figure 2a, CPR spectra of 1L-$ReSe_2$ under right-handed (RCP) and left-handed (LCP) circularly polarized light show clear differences in relative intensities depending on their 2D chirality, which can be explained by the quantum interference effect.[7] In mechanically exfoliated 2L-$ReSe_2$, we find two groups of samples with distinct CPR responses. For Group-I 2L-$ReSe_2$, the CPR spectra show similar features as for 1L-$ReSe_2$ (Figure 2b), and some samples (top row of Figure 2b) show an exactly opposite CPR response to the others (bottom row of Figure 2b), indicating that these 2L-$ReSe_2$ may preserve 2D chirality. The two enantiomers of 2L-$ReSe_2$ are named Group-I 2L-$ReSe_2$(+) and Group-I 2L-$ReSe_2$(−), considering the spectra similarities compared to those of 1L-$ReSe_2$(+) and 1L-$ReSe_2$(−). Interestingly, for Group-II 2L-$ReSe_2$, all of the samples show exactly the same CPR spectra under LCP and RCP excitations (top row of Figure 2c). The circular intensity difference (CID) spectrum under LCP and RCP excitations (I(RCP) − I(LCP)) for Group-II 2L-$ReSe_2$ is presented in Figure S2a, which shows negligible signals compared to the CID spectra of Group-I 2L-$ReSe_2$.

To understand the mechanism for different CPR responses of Group-I and Group-II 2L-$ReSe_2$, we proposed a "CPR signal superposition theory" to qualitatively explain the above phenomena, as shown in Figure 2d. In this theory, the intensity of the CPR spectrum of bilayer $ReSe_2$ can be viewed as the superposition of intensities of individual top and bottom monolayer $ReSe_2$ under the same excitation condition. Therefore, 2L-$ReSe_2$ with EP stacking of two 1L-$ReSe_2$(−) should have a similar CPR spectrum to that of 1L-$ReSe_2$(−) with doubled intensity (top two rows of Figure 2d). In this case, the bilayer still has a chiroptical response, and the CPR intensities depend on the overall 2D chirality. For the racemic-stacked 2L-$ReSe_2$ containing 1L-$ReSe_2$(+) at the top and 1L-$ReSe_2$(−) at the bottom, the spectra of bottom 1L-$ReSe_2$(−) (top 1L-$ReSe_2$(+)) excited by RCP light and top 1L-$ReSe_2$(+) (bottom 1L-$ReSe_2$(−)) excited by LCP light are identical (Figure 2a). Thus, the racemic-stacked 2L-$ReSe_2$ exhibits a negligible chiroptical response with the same CPR intensities under LCP and RCP excitation. Although the real Raman spectrum of bilayer $ReSe_2$ cannot be regarded as the simple superposition of the Raman signals from two monolayers due to the absorption difference, the change of the dielectric environment, and the influence of interlayer van der Waals interaction,[17] this theory qualitatively explains the origin of CPR spectral feature differences between Group-I and Group-II 2L-$ReSe_2$ EP and racemic stacking. Then, we performed annular dark-field (ADF) STEM to examine the atomic structures of Group-I 2L-$ReSe_2$(−) and Group-II 2L-$ReSe_2$. The results are shown in Figure 2e,f, which verifies the stacking order assignment. To test the universality of the as-proposed superposition theory, we also measured the CPR spectra of artificially stacked 2L-$ReSe_2$ with 1L-$ReSe_2$(−) at the top and 1L-$ReSe_2$(+) at the bottom (Figure S2b), and the rotation angle between the ***b***-axis of the top and bottom layers is about 50°, as confirmed by the linear polarized Raman intensity polar plot of mode V^9 (Figure S2c). The CPR spectra of this artificially stacked sample are shown in the bottom row of Figure 2c, which are also identical under LCP and RCP excitations, demonstrating the universality of superposition theory. The above results indicate that the chiroptical properties of 2D chiral crystals can be successfully manipulated by stacking orders with different enantiomer proportions.

For the complete stacking order determination of 2L-$ReSe_2$, the interlayer translation and relative in-plane rotation between the top and bottom layers should also be considered (Figure S3a). The STEM images indicated that the Re-chains (***b***-axis) of the top and bottom layers are nearly parallel for both stackings; therefore, the in-plane rotation angle between the two layers is either ∼0 or ∼180° owing to the C_i symmetry of 1L-$ReSe_2$. As shown in Figure S2d, 2L-$ReSe_2$ in Group-I have negligible SHG intensity, which means that they are center inversion symmetric, while the racemic stacking of Group-II 2L-$ReSe_2$ breaks the inversion symmetry, leading to a strong SHG signal. The SHG intensity of Group-II 2L-$ReSe_2$ has a nearly quadratic dependence on the excitation power with a power index of 1.95 ± 0.03, in agreement with the second-order nonlinear mechanism of the SHG process. Monolayer ReX_2 belongs to the C_i point group; thus, the bilayer ReX_2 with an inversion center must have a 0° interlayer rotation angle (see detailed discussion in Section I in the Supporting Information). Considering the relative displacement between the top and bottom layers observed in STEM images, we concluded that Group-I $ReSe_2$ is AB-stacked. For the stacking order of Group-II $ReSe_2$, we abbreviate it as AB_r stacking, where "r" stands for "racemic." It is worth noting that

https://doi.org/10.1021/acsnano.4c02898
ACS Nano 2024, 18, 13858−13865

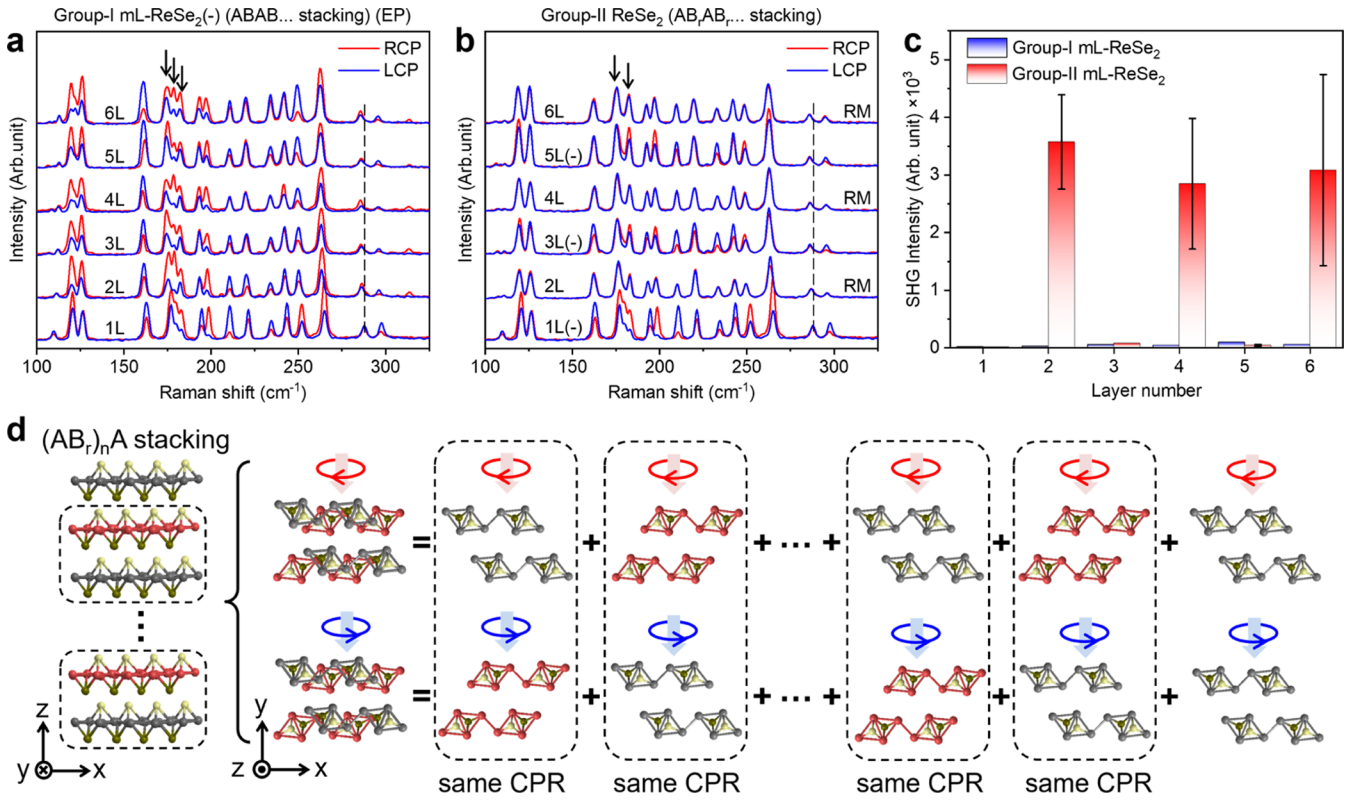

Figure 3. Stacking order determination for multilayer $ReSe_2$. (a, b) Circularly polarized Raman spectra of Group-I (a) and Group-II (b) multilayer $ReSe_2$. (+) and (−) denote for different 2D chirality. Raman peaks with frequencies ranging from 170 to 185 cm^{-1} are marked by arrows. Dashed lines are guides to eyes showing peak frequency differences between samples with different layer numbers. EP, enantiomerically pure; RM, racemic mixture. (c) Layer number dependence of SHG intensity for Group-I and Group-II $ReSe_2$. (d) Schematic diagram of CPR intensity superposition theory for Group-II $ReSe_2$ with odd layer numbers and $(AB_r)_nA$ stacking orders (n = 1, 2, 3, ···). The red (blue) arrows pointing clockwise (anticlockwise) represent RCP (LCP) excitations.

for Group-II $ReSe_2$, the method proposed in this work cannot distinguish whether the interlayer rotation angle is ∼0 or ∼180°, and the vertical relationship of 1L(+) and 1L(−) (which one is at the top and which one is at the bottom) is also unknown. These two problems will be the topics of future works. To demonstrate the universality of our method, we also applied the as-proposed methodology to 2L-ReS_2, and two different stacking orders (AB and AB_z, where "z" denotes ∼180° interlayer rotation around the z-axis) are unambiguously revealed. Detailed discussion can be found in Section IIin the Supporting Information.

Stacking Order Determination of Multilayer $ReSe_2$. Next, we investigated the enantiomer proportions and stacking orders of multilayer (mL) $ReSe_2$. For $ReSe_2$ samples with the same layer number m (m = 2, 3, 4, 5, 6), two different stacking orders are identified, which show distinct CPR responses and different peak numbers from 170 to 185 cm^{-1} (Figure 3a,b). As marked by arrows, these peaks show layer-number-dependent intensity variations, which may be attributed to the changes in multiple reflection interference, electronic band structures, and symmetry of crystallographic structures with different layer numbers.[25,26] Group-I mL-$ReSe_2$ have CPR intensity differences under LCP and RCP excitations regardless of layer number, and only the samples with similar CPR responses as 1L-$ReSe_2$(−) are presented in Figure 3a for clarity. Group-II mL-$ReSe_2$ have no chiroptical response with an even number of layers, and there are weak but distinguishable CPR intensity differences for odd-layer samples (Figure 3b). According to CRP intensity superposition theory, even-layer $ReSe_2$ in Group-II should therefore be regarded as a "racemic mixture" containing an equal number of monolayer 2D enantiomers. The SHG measurement indicates that Group-I mL-$ReSe_2$ with different layer numbers is all inversion symmetric with negligible SHG intensities. Interestingly, for Group-II mL-$ReSe_2$, only even-layer samples show a strong SHG signal, which suggests that the inversion symmetry is broken for even layers but maintained for odd layers.

Now, we try to reveal the stacking orders of mL-$ReSe_2$ from the results presented above. For three-layer $ReSe_2$, both samples in Group-I and Group-II are inversion symmetric; thus, the inversion center should be located at the middle layer, and the top and bottom layers should be inversion symmetric to each other. Therefore, the first and bottom layers must have a 0° interlayer rotation angle and the same 2D chirality (Section I in the Supporting Information). There are two different stacking orders (AB and AB_r) for 2L-$ReSe_2$; thus, it is reasonable to say that the stacking orders of each adjacent layer in mL-$ReSe_2$ should be either AB or AB_r. The above analyses limit the possible stacking orders of three-layer $ReSe_2$ to two possibilities: ABA and AB_rA stackings. In ABA-stacked three-layers, all of the 1L-$ReSe_2$ have the same 2D chirality; therefore, a more distinguishable CPR response is expected, while in AB_rA-stacked three-layers, the bottom and middle layers form a racemic mixture and will not exhibit chiroptical phenomena; thus, it should only have a weak CPR intensity difference under LCP and RCP excitations contributed by the top layer (Figure 3d). The above mechanism can well explain the experimental results of both CPR and SHG if we assign Group-I 3L-$ReSe_2$ as ABA-stacked and Group-II 3L-

https://doi.org/10.1021/acsnano.4c02898
ACS Nano 2024, 18, 13858−13865

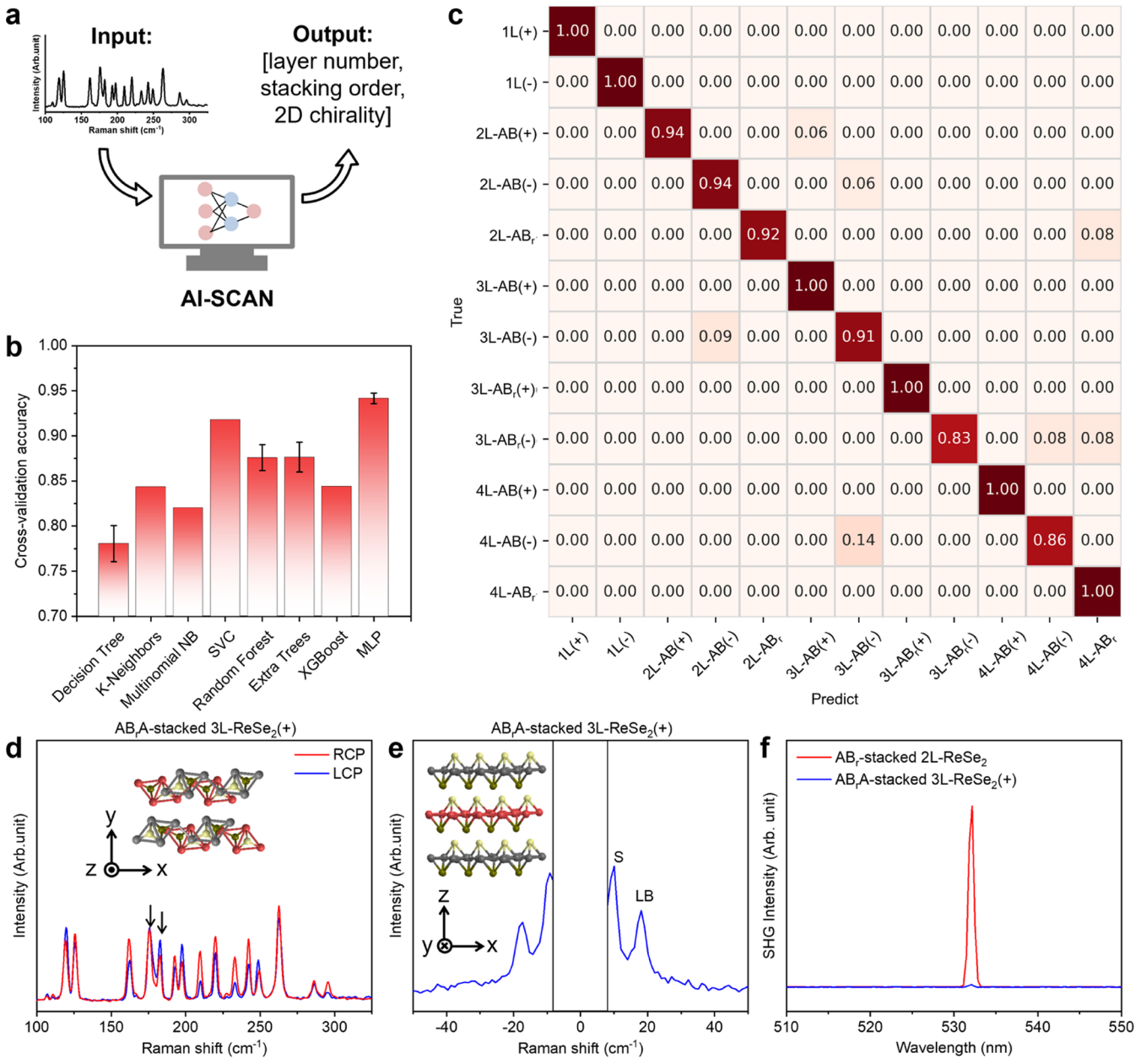

Figure 4. AI Spectra Classification Assistant (AI-SCAN) for crystallographic structure identification. (a) The flowchart of the machine learning procedure for AI-SCAN. The input is a single CPR spectrum of the 2D chiral crystals, and the output is the corresponding structural parameters including layer number, stacking order, and 2D chirality. (b) Statistics of 5-fold cross-validation (CV) accuracies of the testing results using different machine learning models. (c) Confusion matrix calculated from the testing results using MPL as the machine learning model. m-layer ABAB···-stacked $ReSe_2$ with (+) chirality is abbreviated as "mL-AB(+)," while the *n*-layer AB_rAB_r···-stacked $ReSe_2$ racemic mixture is abbreviated as "nL-AB$_r$." Other structures are abbreviated in a similar way. (d) Circularly polarized Raman spectra of an unknown $ReSe_2$ sample, which is predicted to be AB_rA-stacked 3L-$ReSe_2$(+) by AI-SCAN. Raman peaks with frequencies ranging from 170 to 185 cm^{-1} are marked by arrows. (e) Raman spectrum of interlayer shear and layer-breathing modes of the same sample in (d). The insets of parts (d) and (e) depict the simplified crystal structures of AB_rA-stacked 3L-$ReSe_2$(+). (f) SHG spectra of AB_r-stacked 2L-$ReSe_2$ and AB_rA-stacked 3L-$ReSe_2$(+).

$ReSe_2$ as AB_rA-stacked. Notice that both ABA and AB_rA three-layers have overall 2D chirality, and different enantiomers are labeled as 3L-$ReSe_2$(+) and 3L-$ReSe_2$(−) according to the CPR spectral feature similarities compared to 1L-$ReSe_2$(+) and 1L-$ReSe_2$(−).

For four layers, it can be regarded as the stacking of three layers and a monolayer with either AB or AB_r interfaces between the outer layer of 3L-$ReSe_2$ and 1L-$ReSe_2$. Based on the stacking orders of 3L-$ReSe_2$, four-layer $ReSe_2$ has the following four possible stacking orders: ABAB, $ABAB_r$, AB_rAB, and AB_rAB_r. Only the ABAB stacking preserves the inversion center, and only AB_rAB_r is a racemic mixture without a chiroptical response. Therefore, we assigned Group-I 4L-$ReSe_2$ as the ABAB stacking and Group-II 4L-$ReSe_2$ as the AB_rAB_r stacking. Similar analysis can be applied to other odd-layer and even-layer $ReSe_2$, from which we can draw conclusions that Group-I mL-$ReSe_2$ has ABABAB··· stacking and Group-II mL-$ReSe_2$ has $AB_rAB_rAB_r$··· stacking. As for mL-ReS_2, we also found two groups of samples with different stacking orders, and the CPR and SHG results indicate that they are ABABAB··· stacking and $AB_zAB_zAB_z$···

https://doi.org/10.1021/acsnano.4c02898
ACS Nano 2024, 18, 13858−13865

stacking (see detailed discussion in Section III in the Supporting Information).

Machine Learning-Assisted Crystallographic Structure Identification from a Single CPR Spectrum. Finally, we show that a single CPR spectrum is enough to unambiguously identify the structural parameters including layer number, stacking order, and 2D chirality of mechanically exfoliated 2D chiral crystals with the help of a machine learning model. The frequencies of specific Raman modes of ReX_2 have layer number dependence (dashed lines in Figures 3a,b and S6), which can be potentially used to determine the layer number. To distinguish different stacking orders, one can examine the peak numbers (arrows in Figure 3a,b) and frequencies (mode I in Figure S6) of specific Raman modes because they are stacking-order-dependent. As for 2D chirality, the relative CPR peak intensities for different Raman modes under LCP excitation are distinct for mL-ReX_2(+), mL-ReX_2(−), and racemic mixtures. Therefore, the 2D chirality of multilayers can be theoretically identified from a single LCP-excited CPR spectrum, which is also the case for RCP excitations. Unfortunately, all of these complicated spectral features only have subtle differences between samples with different layer numbers, stacking orders, and 2D chirality, which makes the manual identification of these structural parameters laborious and inaccurate.

To address this problem, we trained an AI Spectra Classification Assistant (AI-SCAN) with a single LCP-excited CPR spectrum as input and the above structural parameters as output (Figure 4a). The true layer number, stacking order, and 2D chirality of $ReSe_2$ samples in training data were determined by the systematic experimental characterization combining CPR, SHG, and STEM, as proposed in Figures 2 and 3. Figure 4b shows the training results for mL-$ReSe_2$ evaluated by 5-fold cross-validation (CV) accuracy. Different machine learning models are tested, which include decision tree, K-nearest neighbors (K-neighbors), multinomial Naive Bayes (NB), support vector classification (SVC), random forest, extremely randomized trees (extra trees), extreme gradient boosting (XGBoost), and multilayer perceptron (MLP). We selected MLP as the basis for our AI Spectra Classification Assistant because it exhibited the highest CV accuracy score of 0.9417 ± 0.0059. Then, we analyzed the prediction accuracy of each class of mL-$ReSe_2$ using a confusion matrix, as shown in Figure 4c. The diagonal elements are the success rates of each class, while the off-diagonal elements are the rates of misclassified spectra. The classification accuracies of $ReSe_2$ with different structural parameters are all above 80%, and half of the structure classes have prediction accuracies reaching 100%.

To further examine the accuracy of AI-SCAN, we randomly selected a sample that is never input to MLP. By inputting its LCP-excited CPR spectrum (Figure 4d) to AI-SCAN, the model outputs the predicted structural parameters as AB_rA-stacked 3L-$ReSe_2$(+). We then applied the crystallographic structure determination methodology proposed in Figures 2 and 3 to check the true layer number, stacking order, and 2D chirality of this sample. As shown in Figure 4d, there are only two Raman peaks in the range of 170−185 cm^{-1}, indicating an $AB_rAB_r\cdots$ stacking order. The CPR response is opposite that of $AB_rAB_r\cdots$-stacked $ReSe_2$(−) shown in Figure 3b, which means that the 2D chirality of this sample is "(−)." The frequencies of interlayer shear (S) and layer-breathing (LB) modes indicate that the layer number is three.[24] Thus, this sample is indeed an AB_rA-stacked 3L-$ReSe_2$(+), and its inversion center is reserved with no SHG intensity compared to AB_r-stacked 2L-$ReSe_2$ (Figure 4f), agreeing well with the results in Figure 3c. All of the above results indicate that AI-SCAN realizes the potential of CPR spectroscopy as a powerful tool to identify the structural parameters of 2D chiral crystals.

CONCLUSIONS

In conclusion, we demonstrated that the enantiomer proportion and stacking order degrees of freedom can be exploited to effectively manipulate the chiral Raman response of 2D chiral crystals. With a comprehensive analysis using CPR, SHG, and STEM, the stacking orders of multilayer $ReSe_2$ and ReS_2 are unambiguously elaborated. Based on the above knowledge, we developed an AI Spectra Classification Assistant, which can identify the layer number, stacking order, and 2D chirality from a single CPR spectrum. The chirality manipulation and crystallographic structure determination methodologies proposed in this work can also be applied to other 2D chiral crystals such as 1T-TaS_2 with chiral charge density waves, which may facilitate the discoveries of other stacking order-related chiral properties such as chiral stacking-dependent sliding ferroelectricity.[19] It is worth noting that the AI-SCAN proposed in this work was trained only based on the data of the $ReSe_2$ sample with ABAB··· and $AB_rAB_r\cdots$ stackings; thus, the model is only valid for samples with crystallographic structures mentioned in this work. To improve the generalizability of AI-SCAN, the training data of CPR and structure parameters from $ReSe_2$ with different stacking orders or other 2D chiral crystals will be welcomed in future works. Besides, the key factor governing the thermodynamic stability of different stackings is also worth exploring. In this work, we investigated 102 2L-$ReSe_2$ samples, with 85 AB-stacked and 17 AB_r-stacked. For ReS_2, we also investigated 102 bilayer samples; 88 of them are AB-stacked and 14 of them are AB_z-stacked. Therefore, the most stable stacking order for both ReS_2 and $ReSe_2$ is AB stacking, but the metastable stacking orders for ReS_2 and $ReSe_2$ are different. Future works are welcomed to explain this phenomenon and the outcomes may instruct the scalable synthesis of 2D chiral crystals with designable stacking order and enantiomer proportion.

EXPERIMENTAL SECTION

Raman Measurement. Raman spectra were measured at room temperature using a JY Horiba HR800 (1800 lines/mm grating, 2.33 and 1.96 eV excitation) or a WITec α 300RSA (2400 lines/mm grating, 2.54 eV excitation), both of which were equipped with a × 100 objective lens (numerical aperture = 0.90). The laser power was kept below 0.3 mW to avoid damage to samples. All CPR spectra were measured under 2.33 eV excitation with the same optical setup as in the previous report.[7]

SHG Measurement. SHG spectra were measured at room temperature using a WITec α 300R with a 150 lines/mm grating and a ×100 objective lens (numerical aperture = 0.90). A linearly polarized picosecond laser (15 ps, 50 MHz) with a wavelength of 1064 nm was used.

STEM Measurement. Polypropylene carbonate (PPC, M_n = 50,000 g/mol) and benzaldehyde were purchased from Sigma-Aldrich (Shanghai, China). The 2L-ReX_2 sample on the 90 nm SiO_2/Si substrate was first spin-coated with PPC in benzaldehyde (0.15 g/mL) at 2500 rpm (45 s) and then baked at 80 °C (1 min). The PPC/ReX_2 film was detached from the 90 nm SiO_2/Si substrate with the aid of a water droplet and then placed on a holey carbon TEM grid with an array of holes 600 nm in diameter. The temperature was raised to 110 °C until the sample and the grid were well in contact. Finally, the PPC/ReX_2/grid was placed in acetone for 12 h at room temperature to remove the PPC.

Atomic-resolution ADF-STEM imaging was performed on a probe-corrected scanning transition electron microscope (Titan Cubed

https://doi.org/10.1021/acsnano.4c02898
ACS Nano 2024, 18, 13858−13865

Themis G2 200) operated at an accelerating voltage of 300 kV. The convergence semiangle of the probe was set to 30 mrad, and the collection semiangle for ADF-STEM was in the range of 39−200 mrad. Pristine ADF-STEM images were filtered by Gaussian filters to improve the signal-to-noise ratio for a better display.

Software and Machine Learning. All algorithms in this work were written with Python in Jupyter notebooks using the following libraries: Pandas 1.0.5, Numpy 1.18.5, Matplotlib 3.2.2, Seaborn 0.10.1, and Scikit-learn 0.23.1. 134 $ReSe_2$ samples with layer numbers ranging from one to four were used as either a training set or a testing set for machine learning. The 1800 lines per mm grating of the JY Horiba HR800 enables each CCD pixel to cover 0.5 cm^{-1} at 2.33 eV. The spectral ranges of 103−135 and 155−304 cm^{-1} were used, which include 332 CCD pixels. The 332 Raman intensities values at these pixels were used as input features. The intensity value at each pixel was normalized so that the 134 intensity values at this pixel from all of the samples satisfied the standard normal distribution. The combinations of different layer numbers, stacking order, and 2D chirality yielded 12 different possible $ReSe_2$ structures, which were labeled from 0 to 11 and used as the output of the classification task. During the 5-fold CV, the data set underwent five different train/test splits. In each split, 80% of the data were used as a training set, and 20% of the data were used as a testing set. The final CV accuracy was the average of the prediction accuracies of the five splits. We optimized the hyperparameters of all models based on the 5-fold CV accuracy values. The optimized hyperparameters of all models can be found in Section IV in the Supporting Information.

ASSOCIATED CONTENT

Data Availability Statement

All data are available in the main text or in the Supporting Information and are available from the corresponding authors upon reasonable request.

Supporting Information

The Supporting Information is available free of charge at https://pubs.acs.org/doi/10.1021/acsnano.4c02898.

Section I, relationship among the interlayer rotation angle, 2D chirality, and inversion symmetry for 2L-ReX_2; Section II, enantiomer proportion and stacking order determination of bilayer ReS_2; Section III, stacking orders of mL-ReS_2; Section IV, optimized hyperparameters for machine learning models; Figures S1−S6, low-frequency Raman spectra for interlayer modes of multilayer ReS_2 and $ReSe_2$ under 2.54 eV excitation; supplementary experimental evidence for stacking order determination of 2L-$ReSe_2$; schematic diagram for complete stacking order determination; enantiomer proportions and stacking orders of 2L-ReS_2; supplementary experimental evidence for stacking order determination of 2L-ReS_2; and stacking order determination for multilayer ReS_2 (PDF)

Python code of the machine learning procedure for AI-SCAN (ZIP)

AUTHOR INFORMATION

Corresponding Author

Lianming Tong − *Center for Nanochemistry, Beijing Science and Engineering Center for Nanocarbons, Beijing National Laboratory for Molecular Sciences, College of Chemistry and Molecular Engineering, Peking University, 100871 Beijing, China;* orcid.org/0000-0001-7771-4077; Email: tonglm@pku.edu.cn

Authors

He Hao − *Center for Nanochemistry, Beijing Science and Engineering Center for Nanocarbons, Beijing National Laboratory for Molecular Sciences, College of Chemistry and Molecular Engineering, Peking University, 100871 Beijing, China*

Kangshu Li − *School of Materials Science and Engineering, Peking University, 100871 Beijing, China*

Xujing Ji − *School of Materials Science and Engineering, Peking University, 100871 Beijing, China*

Xiaoxu Zhao − *School of Materials Science and Engineering, Peking University, 100871 Beijing, China;* orcid.org/0000-0001-9746-3770

Jin Zhang − *Center for Nanochemistry, Beijing Science and Engineering Center for Nanocarbons, Beijing National Laboratory for Molecular Sciences, College of Chemistry and Molecular Engineering, Peking University, 100871 Beijing, China; School of Advanced Materials, Peking University Shenzhen Graduate School, 518055 Shenzhen, Guangdong, China;* orcid.org/0000-0003-3731-8859

Complete contact information is available at: https://pubs.acs.org/10.1021/acsnano.4c02898

Author Contributions

H.H. performed the Raman and SHG measurements and wrote the machine learning algorithm. K.L. and X.J. performed the STEM measurement. X.Z. supervised the STEM measurement. L.T. and J.Z. supervised all the experiments and data collection. All authors contributed to the discussion of data and writing of the manuscript.

Notes

The authors declare no competing financial interest.

Code availability All codes used for the analysis of this study are available from the corresponding authors upon reasonable request.

ACKNOWLEDGMENTS

This work was financially supported by the Ministry of Science and Technology of China (2022YFA1203302, 2022YFA1203304, and 2018YFA0703502), the National Natural Science Foundation of China (Grant Nos. 52021006, 21974004, and 52273279), the Strategic Priority Research Program of CAS (XDB36030100), the Beijing Natural Science Foundation (Grant No. Z220020), the Fundamental Research Funds for the Central Universities and the Beijing National Laboratory for Molecular Sciences (BNLMS-CXTD-202001), and the Shenzhen Science and Technology Innovation Commission (KQTD20221101115627004). The authors acknowledge Electron Microscopy Laboratory of Peking University, China, for the use of Cs corrected Titan Cubed Themis G2 200 transmission electron microscopy.

REFERENCES

(1) Peluso, P.; Chankvetadze, B. Recognition in the Domain of Molecular Chirality: From Noncovalent Interactions to Separation of Enantiomers. *Chem. Rev.* **2022**, *122*, 13235−13400.

(2) Liu, M. H.; Zhang, L.; Wang, T. Y. Supramolecular Chirality in Self-Assembled Systems. *Chem. Rev.* **2015**, *115*, 7304−7397.

(3) Naaman, R.; Paltiel, Y.; Waldeck, D. H. Chiral Molecules and the Electron Spin. *Nat. Rev. Chem.* **2019**, *3*, 250−260.

(4) Yang, S. H.; Naaman, R.; Paltiel, Y.; Parkin, S. S. P. Chiral Spintronics. *Nat. Rev. Phys.* **2021**, *3*, 328−343.

(5) Mun, J.; Kim, M.; Yang, Y.; Badloe, T.; Ni, J. C.; Chen, Y.; Qiu, C. W.; Rho, J. Electromagnetic Chirality: From Fundamentals to Nontraditional Chiroptical Phenomena. *Light: Sci. Appl.* **2020**, *9*, 139.

(6) Klein, D. R. *Organic Chemistry*, 1st ed.; John Wiley & Sons, Inc., 2012.
(7) Zhang, S. S.; Huang, J. Q.; Yu, Y.; Wang, S. S.; Yang, T.; Zhang, Z. D.; Tong, L. M.; Zhang, J. Quantum Interference Directed Chiral Raman Scattering in Two-Dimensional Enantiomers. *Nat. Commun.* **2022**, *13*, No. 1254.
(8) Hart, L.; Dale, S.; Hoye, S.; Webb, J. L.; Wolverson, D. Rhenium Dichalcogenides: Layered Semiconductors with Two Vertical Orientations. *Nano Lett.* **2016**, *16*, 1381−1386.
(9) Choi, Y.; Kim, K.; Lim, S. Y.; Kim, J.; Park, J. M.; Kim, J. H.; Lee, Z.; Cheong, H. Complete Determination of the Crystallographic Orientation of ReX_2 (X = S, Se) by Polarized Raman Spectroscopy. *Nanoscale Horiz.* **2020**, *5*, 308−315.
(10) Zhao, Y.; Nie, Z. W.; Hong, H.; Qiu, X.; Han, S. Y.; Yu, Y.; Liu, M. X.; Qiu, X. H.; Liu, K. H.; Meng, S.; Tong, L. M.; Zhang, J. Spectroscopic Visualization and Phase Manipulation of Chiral Charge Density Waves in 1T-TaS_2. *Nat. Commun.* **2023**, *14*, No. 2223.
(11) Fichera, B. T.; Kogar, A.; Ye, L. D.; Gökce, B.; Zong, A.; Checkelsky, J. G.; Gedik, N. Second Harmonic Generation as a Probe of Broken Mirror Symmetry. *Phys. Rev. B* **2020**, *101*, 241106R.
(12) Yang, H. F.; He, K. Y.; Koo, J.; Shen, S. W.; Zhang, S. H.; Liu, G.; Liu, Y. Z.; Chen, C.; Liang, A. J.; Huang, K.; Wang, M. X.; Gao, J. J.; Luo, X.; Yang, L. X.; Liu, J. P.; Sun, Y. P.; Yan, S. C.; Yan, B. H.; Chen, Y. L.; Xi, X.; Liu, Z. K. Visualization of Chiral Electronic Structure and Anomalous Optical Response in a Material with Chiral Charge Density Waves. *Phys. Rev. Lett.* **2022**, *129*, No. 156401.
(13) Zong, A.; Shen, X. Z.; Kogar, A.; Ye, L. D.; Marks, C.; Chowdhury, D.; Rohwer, T.; Freelon, B.; Weathersby, S.; Li, R. K.; Yang, J.; Checkelsky, J.; Wang, X. J.; Gedik, N. Ultrafast Manipulation of Mirror Domain Walls in a Charge Density Wave. *Sci. Adv.* **2018**, *4*, No. eaau5501.
(14) Fedotov, V. A.; Mladyonov, P. L.; Prosvirnin, S. L.; Rogacheva, A. V.; Chen, Y.; Zheludev, N. I. Asymmetric Propagation of Electromagnetic Waves through a Planar Chiral Structure. *Phys. Rev. Lett.* **2006**, *97*, No. 167401.
(15) Tongay, S.; Sahin, H.; Ko, C.; Luce, A.; Fan, W.; Liu, K.; Zhou, J.; Huang, Y. S.; Ho, C. H.; Yan, J. Y.; Ogletree, D. F.; Aloni, S.; Ji, J.; Li, S. S.; Li, J. B.; Peeters, F. M.; Wu, J. Q. Monolayer Behaviour in Bulk ReS_2 Due to Electronic and Vibrational Decoupling. *Nat. Commun.* **2014**, *5*, No. 3252.
(16) He, R.; Yan, J. A.; Yin, Z. Y.; Ye, Z. P.; Ye, G. H.; Cheng, J.; Li, J.; Lui, C. H. Coupling and Stacking Order of ReS_2 Atomic Layers Revealed by Ultralow-Frequency Raman Spectroscopy. *Nano Lett.* **2016**, *16*, 1404−1409.
(17) Qiao, X. F.; Wu, J. B.; Zhou, L. W.; Qiao, J. S.; Shi, W.; Chen, T.; Zhang, X.; Zhang, J.; Ji, W.; Tan, P. H. Polytypism and Unexpected Strong Interlayer Coupling in Two-Dimensional Layered ReS_2. *Nanoscale* **2016**, *8*, 8324−8332.
(18) Zhou, Y. J.; Maity, N.; Rai, A.; Juneja, R.; Meng, X. H.; Roy, A.; Zhang, Y. Y.; Xu, X. C.; Lin, J. F.; Banerjee, S. K.; Singh, A. K.; Wang, Y. G. Stacking-Order-Driven Optical Properties and Carrier Dynamics in ReS_2. *Adv. Mater.* **2020**, *32*, No. 1908311.
(19) Wan, Y.; Hu, T.; Mao, X. Y.; Fu, J.; Yuan, K.; Song, Y.; Gan, X. T.; Xu, X. L.; Xue, M. Z.; Cheng, X.; Huang, C. X.; Yang, J. B.; Dai, L.; Zeng, H. L.; Kan, E. J. Room-Temperature Ferroelectricity in 1T'-ReS_2 Multilayers. *Phys. Rev. Lett.* **2022**, *128*, No. 067601.
(20) Van der Laan, M.; Heemskerk, E.; Kienhuis, F.; Diepeveen, N.; Poonia, D.; Kinge, S.; Dang, M. T.; Dinh, V.; Siebbeles, L. D. A.; Isaeva, A.; van de Groep, J.; Schall, P. Stacking-Order-Dependent Excitonic Properties Reveal Interlayer Interactions in Bulk ReS_2. *ACS Photonics* **2023**, *10*, 3115−3123.
(21) Song, Y.; Shan, Y. W.; Wang, W. M.; Chang, K. A.; Zheng, Z.; Shi, Z. M.; Li, D. B.; Cheng, J. L. Second Harmonic Generation in Exfoliated Few-Layer ReS_2. *Adv. Opt. Mater.* **2023**, *11*, No. 2300111.
(22) Dhakal, K. P.; Kim, H.; Lee, S.; Kim, Y.; Lee, J.; Ahn, J. H. Probing the Upper Band Gap of Atomic Rhenium Disulfide Layers. *Light: Sci. Appl.* **2018**, *7*, 98.
(23) Song, Y.; Hu, S. Q.; Lin, M. L.; Gan, X. T.; Tan, P. H.; Zhao, J. L. Extraordinary Second Harmonic Generation in ReS_2 Atomic Crystals. *ACS Photonics* **2018**, *5*, 3485−3491.
(24) Lorchat, E.; Froehlicher, G.; Berciaud, S. Splitting of Interlayer Shear Modes and Photon Energy Dependent Anisotropic Raman Response in *N*-Layer $ReSe_2$ and ReS_2. *ACS Nano* **2016**, *10*, 2752−2760.
(25) McCreary, A.; Simpson, J. R.; Wang, Y. X.; Rhodes, D.; Fujisawa, K.; Balicas, L.; Dubey, M.; Crespi, V. H.; Terrones, M.; Walker, A. R. H. Intricate Resonant Raman Response in Anisotropic ReS_2. *Nano Lett.* **2017**, *17*, 5897−5907.
(26) Arora, A.; Noky, J.; Drüppel, M.; Jariwala, B.; Deilmann, T.; Schneider, R.; Schmidt, R.; Del Pozo-Zamudio, O.; Stiehm, T.; Bhattacharya, A.; Krüger, P.; de Vasconcellos, S. M.; Rohlfing, M.; Bratschitsch, R. Highly Anisotropic in-Plane Excitons in Atomically Thin and Bulklike 1T′-$ReSe_2$. *Nano Lett.* **2017**, *17*, 3202−3207.

https://doi.org/10.1021/acsnano.4c02898
ACS Nano 2024, 18, 13858−13865